

# D-81519 OCO-2 Algorithm Theoretical Basis Document

## IMAP-DOAS preprocessor

Christian Frankenberg (CF)  
Jet Propulsion Laboratory, California Institute of Technology, Pasadena, USA.

2014-04-01

### Revision History

<b>Revision</b>	<b>Date</b>	<b>Author(s)</b>	<b>Description</b>
1.0	01.04.2014	CF	initial version created

# Contents

<b>1</b>	<b>Introduction</b>	<b>3</b>
<b>2</b>	<b>CO<sub>2</sub> and H<sub>2</sub>O non-scattering retrievals for cloud and aerosol screening</b>	<b>3</b>
2.1	Vertical Column Density retrievals in single-band mode . . . . .	5
<b>3</b>	<b>Solar Induced Fluorescence (SIF) retrievals</b>	<b>5</b>

## 1 Introduction

The primary science goal of the National Aeronautics and Space Administration’s (NASA) Orbiting Carbon Observatory-2 (OCO-2) satellite is to allow for the quantification of global sources and sinks of atmospheric carbon dioxide ( $\text{CO}_2$ ) by providing high spectral resolution near-infrared (IR) measurements of reflected solar light Crisp et al. (2004). The radiance measurements of backscattered sunlight in the  $0.76 \mu\text{m}$   $\text{O}_2$  A-band the  $2.06 \mu\text{m}$  and  $1.61 \mu\text{m}$  strong and weak  $\text{CO}_2$  bands will be made in three science observation modes (nadir, glint and target) at spatial and temporal resolutions much higher than are currently available from other satellite systems Crisp and Johnson (2005).

The high spectral resolution of the OCO-2 measurements will provide the necessary sensitivity to the sources and sinks of  $\text{CO}_2$  found near the earth’s surface, while simultaneously minimizing systematic measurement errors. The high spatial and temporal sampling will provide 8 IFOV footprints per 3 Hz frame, each footprint at  $\simeq 1.3 \text{ km}$  cross track and  $\simeq 2.3 \text{ km}$  along-track. The instrument functions only on the day light side of the orbit, yielding approximately 35k soundings per orbit ( $\simeq 1$  million per day).

A sounding selector tool will be used to determine the exact soundings that will be processed by the computationally expensive Level 2  $X_{\text{CO}_2}$  retrieval algorithm Mandrake et al. (2013). The L2 algorithm is a Bayesian retrieval that produces estimates of  $X_{\text{CO}_2}$ , as well as other state variable values, given the high spectral resolution radiances as inputs O’Dell et al. (2012) and Crisp et al. (2012). Current computational speeds and budget limitations dictate that approximately 6-7% of the total number of collected soundings will be processed by L2.

One of the largest drivers of error in the retrieval algorithm is scattering due to cloud and aerosol, which adds uncertainties to the radiance measurements, and hence to the retrieved  $X_{\text{CO}_2}$ . Screening of contaminated scenes is therefore required in order to maximize the data yield. Although atmospheric scattering is accounted for in the L2 code, scenes with total optical thicknesses of more than  $\simeq 0.3$  yield erroneous retrievals of  $X_{\text{CO}_2}$ , or outright failure of the algorithm.

In addition, it has been recognized that solar induced fluorescence (SIF) can be retrieved from OCO-2 spectra and will provide a very useful product for global carbon cycle research.

This document describes in detail the so-called IMAP-DOAS preprocessor, which is used for both screening of the official  $X_{\text{CO}_2}$  product as well as for the retrieval of SIF from the  $0.76 \mu\text{m}$   $\text{O}_2$  A-band. The IMAP-DOAS preprocessor, just as the ABO2 cloud screen, is implemented in the operational OCO-2 processing pipeline.

## 2 $\text{CO}_2$ and $\text{H}_2\text{O}$ non-scattering retrievals for cloud and aerosol screening

This section describes the use of single-band non-scattering retrievals of  $\text{CO}_2$  and  $\text{H}_2\text{O}$  in the  $2.06 \mu\text{m}$  (strong band, abbreviated by  $S$ ) and  $1.61 \mu\text{m}$  (weak band, abbreviated by  $W$ ) bands, respectively. The basic idea behind using single band non-scattering retrievals for screening purposes is that, in the limit of a non-scattering atmosphere, both bands should agree with each other. Scattering in the atmosphere, however, will affect the  $2.06 \mu\text{m}$  and

1.61  $\mu$ mbands differently because the absorption strength as well as the surface albedos in both bands differ. This causes a divergence of  $\text{CO}_2$  and  $\text{H}_2\text{O}$  as retrieved in both bands independently. This was confirmed using GOSAT measurements (Mandrake et al., 2013) as well using OCO-2 orbit simulations and we found that it is a very sensitive indicator for scattering even in scenes that would be flagged as cloud-free in the ABO2 cloud screen algorithm.

Denoting the retrieved vertical column densities (VCD) of  $\text{CO}_2$  retrieved in the weak and strong bands as  $\text{VCD}_{W\text{CO}_2}$  and  $\text{VCD}_{S\text{CO}_2}$ , respectively, we define the  $\text{CO}_2$  and  $\text{H}_2\text{O}$  ratios as:

$$R_{\text{CO}_2} = \frac{\text{VCD}_{W\text{CO}_2}}{\text{VCD}_{S\text{CO}_2}},$$

and

$$R_{\text{H}_2\text{O}} = \frac{\text{VCD}_{W\text{H}_2\text{O}}}{\text{VCD}_{S\text{H}_2\text{O}}}.$$

$R_{\text{CO}_2}$  is the main quantity used for sounding selection in Mandrake et al. (2013), with lower and upper boundaries set for respective warn levels.  $R_{\text{H}_2\text{O}}$  should be used with caution as it can be noisy in very dry regions and sensitivity of the weak and strong band can differ more strongly than for  $\text{CO}_2$ .

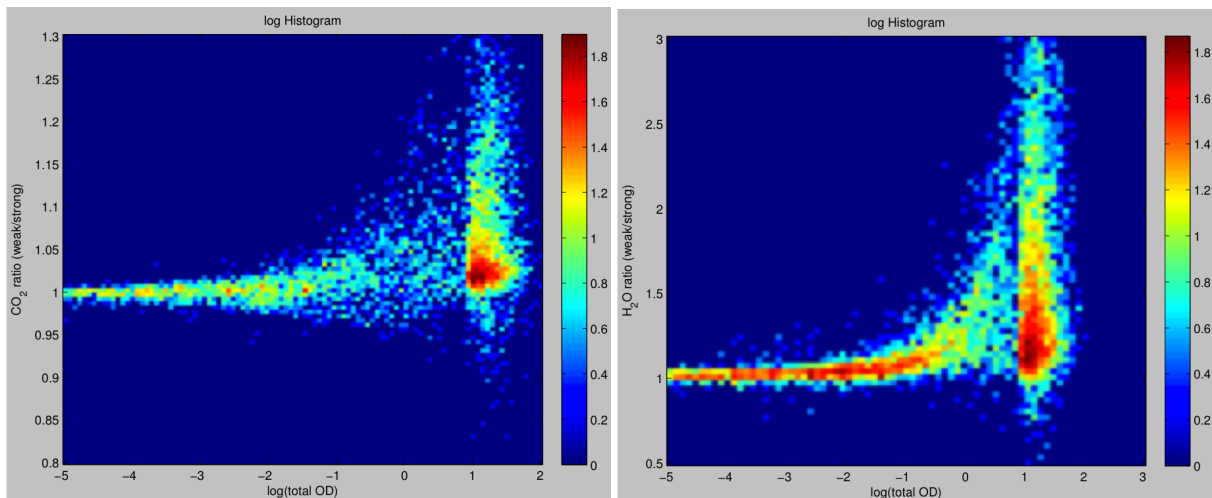


Figure 1: Examples of the dependence of the  $\text{CO}_2$  (left) and  $\text{H}_2\text{O}$  ratios as a function of the natural logarithm of the total optical density in the scene (using GOSAT orbit simulations). The colors indicate the frequency (in log-scale) of samples within the specific area as obtained from the orbit simulator (for which true optical thickness is known). By setting tight upper and lower boundary thresholds for the  $\text{CO}_2$  ratio, most of the higher optical thicknesses can be easily filtered out.

In the following, we will briefly describe the algorithms to derive  $\text{VCD}_{W\text{CO}_2}$  and  $\text{VCD}_{S\text{CO}_2}$  (same for  $\text{H}_2\text{O}$ ).

## 2.1 Vertical Column Density retrievals in single-band mode

The non-scattering retrievals of VCDs in both the weak and the strong band are based on the Iterative Maximum A Posteriori DOAS approach described in Frankenberg et al. (2005). In both retrieval windows, CO<sub>2</sub> and H<sub>2</sub>O are fitted as main absorbers. For H<sub>2</sub>O, we use the co-located ECMWF forecast as a priori and scale the profile without hard constraints. For CO<sub>2</sub>, we use a constant prior of 380 ppm in the troposphere, decreasing to 370 ppm at 60 km. To increase computational speed, we also scale the entire CO<sub>2</sub> profile but have the flexibility to switch to a full profile retrieval. The state vector comprises the respective CO<sub>2</sub> and H<sub>2</sub>O vertical columns, a second order polynomial for wavelength calibration, a spectral shift of the Fraunhofer lines with respect to atmospheric absorption features and a second order polynomial for the broad-band reflectance spectral shape. Elevation corrected surface pressure and pressure/humidity profiles used as a priori are identical to the one being used for the full-physics XCO<sub>2</sub> retrieval, using ECMWF as meteorological input and a high resolution topographic map for elevation correction of input profiles. Airmass factors depending on solar and viewing zenith angles are calculated geometrically with corrections for sphericity adapted from Kasten and Young (1989).

For spectroscopy, the IMAP-DOAS code utilizes the ABSCO cross section data-tables (used for the full-physics retrievals) converted to a proprietary binary format for heritage reasons. Foreign broadening with water vapor is ignored but self-broadening of H<sub>2</sub>O lines is empirically included, assuming a 5-times higher self-broadening coefficient compared to air-broadening for H<sub>2</sub>O.

In principle, the IMAP-DOAS retrieval code is very similar to the full-physics retrievals except for the forward model, which entirely ignores scattering. Apart from that, the inversion scheme is also based on non-linear Optimal Estimation but doesn't use Levenberg-Marquardt solvers as the problem is sufficiently stable. For the full-physics retrievals, radiative transfer is the most time limiting factor, which is not the case for the IMAP-DOAS code. Based on its heritage with SCIAMACHY and GOSAT retrievals, it is highly optimized for speed, fully implemented in C++, and can process about 100 single band retrievals per second.

Eventually, the CO<sub>2</sub> ratios as calculated in IMAP-DOAS are used (among other factors) to select soundings to be passed to the L2 retrieval as described in Mandrake et al. (2013).

## 3 Solar Induced Fluorescence (SIF) retrievals

As has been recognized by Joiner et al. (2011) and Frankenberg et al. (2011a,b), solar induced fluorescence can be retrieved from high-resolution spectra of the O<sub>2</sub> A-band by using micro-windows consisting primarily of solar Fraunhofer lines. The algorithm described in detail in Frankenberg et al. (2011a,b) has been implemented for OCO-2 retrievals and is running using the IMAP-DOAS codebase, controlled by external (ASCII) parameter files defining fit parameters and input data. Further details can be found in Frankenberg et al. (2012) and Frankenberg et al. (2014).

For OCO-2, we are using two separate microwindows for SIF retrievals, centered around 758 nm and 770 nm. The retrievals uses a very simple forward model, based on a high resolution solar transmission spectrum  $\vec{I}_0$ , a relative fluorescence contribution  $F_s^{rel}$  and

polynomial coefficients  $a_i$  to account for the spectral shape of the measured radiance:

$$\vec{f}(F_s^{rel}, a) = \log \left( \langle \vec{I}_0 + F_s^{rel} \rangle \right) + \sum_{i=0}^n a_i \cdot \lambda^i, \quad (1)$$

where the  $\langle \rangle$  operator denotes the convolution (and sampling) with the OCO-2 spectral response function and subsequent sampling for each detector pixel. We also include O<sub>2</sub> absorptions in the forward model and fit as these impact both retrieval windows (the 758 nm range is affected by the far wings of the strong O<sub>2</sub> band and the 770 nm fit window includes some weak oxygen absorption features).

The primary retrieved quantities are  $F_{s755}^{rel}$  and  $F_{s771}^{rel}$ , for the 758 and 770 nm microwindow, respectively. These are relative contributions of SIF to the continuum level radiance and will be converted to absolute SIF radiances by using the average continuum level radiance  $I_{cont}$  within each microwindow:

$$SIF_{758} = F_{s755}^{rel} \cdot I_{cont,758}.$$

This computation is performed in a post-processing script, not in the original IMAP code. It should be noted that OCO-2 radiances are reported as  $(I - Q)/2$  (Stokes vector). For unpolarized scenes, as can be mostly expected over land and low scattering, this can be converted to unpolarized full intensities by multiplying with a factor 2 (see Frankenberg et al. (2012) for detail on OCO-2 specific SIF aspects).

There is one caveat regarding the accuracy of absolute SIF radiances: Owing to minor uncertainties in the OCO-2 spectral response function or the solar model used in the fitting routine,  $F_s^{rel}$  can be biased high or low, with slightly different biases in each of the 8 OCO-2 footprints. If uncorrected (which will be the case very early in the mission), a constant bias in  $F_s^{rel}$  will propagate into an intensity-dependent bias in SIF. We will determine the bias values  $c_i$  for each footprint  $i$  using non-vegetated areas, such as deserts, snow, ice or land surfaces with surface temperatures well below freezing. The corrected SIF values would read

$$SIF_{758}^{corr} = (F_{s755}^{rel} - c_i) \cdot I_{cont,758},$$

using a separate  $c_i$  for each of the 8 OCO-2 footprints and wavelength region.

We anticipate to also run the SVD-based fluorescence retrieval (?) in a non-operational stream and have implemented a python prototype that was used for SIF retrievals from synthetic OCO-2 spectra (Frankenberg et al., 2012).

## References

- Crisp, D. and C. Johnson, 2005: The Orbiting Carbon Observatory mission. *J. Atmos. Sci.*, **56**, 193–197, doi:10.1016/j.actaastro.2004.09.032.
- Crisp, D., et al., 2004: The Orbiting Carbon Observatory (OCO) mission. *Adv. Space Res.*, **34**, 700–709, doi:10.1016/j.asr.2003.08.062.
- Crisp, D., et al., 2012: The ACOS CO<sub>2</sub> retrieval algorithm—part II: Global X<sub>CO<sub>2</sub></sub> data characterization. *Atmos. Meas. Tech.*, **5**, 687–707, doi:10.5194/amt-5-687-2012.

- Frankenberg, C., A. Butz, and G. C. Toon, 2011a: Disentangling chlorophyll fluorescence from atmospheric scattering effects in O-2 A-band spectra of reflected sun-light. *Geophysical Research Letters*, **38**, L03 801.
- Frankenberg, C., C. O'Dell, J. Berry, L. Guanter, J. Joiner, P. Köhler, R. Pollock, and T. E. Taylor, 2014: Prospects for chlorophyll fluorescence remote sensing from the orbiting carbon observatory-2. *Remote Sensing of Environment*, **147** (0), 1 – 12, doi:<http://dx.doi.org/10.1016/j.rse.2014.02.007>, URL <http://www.sciencedirect.com/science/article/pii/S0034425714000522>.
- Frankenberg, C., C. O'Dell, L. Guanter, and J. McDuffie, 2012: Remote sensing of near-infrared chlorophyll fluorescence from space in scattering atmospheres: implications for its retrieval and interferences with atmospheric CO<sub>2</sub> retrievals. *Atmospheric Measurement Techniques*, **5** (8), 2081–2094.
- Frankenberg, C., U. Platt, and T. Wagner, 2005: Iterative maximum a posteriori (imap)-doas for retrieval of strongly absorbing trace gases: Model studies for ch<sub>4</sub> and co<sub>2</sub> retrieval from near infrared spectra of sciamachy onboard envisat. *Atmospheric Chemistry and Physics*, **5** (1), 9–22, doi:10.5194/acp-5-9-2005, URL <http://www.atmos-chem-phys.net/5/9/2005/>.
- Frankenberg, C., et al., 2011b: New global observations of the terrestrial carbon cycle from GOSAT: Patterns of plant fluorescence with gross primary productivity. *Geophysical Research Letters*, **38** (17), L17 706.
- Joiner, J., Y. Yoshida, A. P. Vasilkov, Y. Yoshida, L. A. Corp, and E. M. Middleton, 2011: First observations of global and seasonal terrestrial chlorophyll fluorescence from space. *Biogeosciences*, **8** (3), 637–651, doi:10.5194/bg-8-637-2011, URL <http://www.biogeosciences.net/8/637/2011/>.
- Kasten, F. and A. T. Young, 1989: Revised optical air mass tables and approximation formula. *Appl. Opt.*, **28** (22), 4735–4738, doi:10.1364/AO.28.004735, URL <http://ao.osa.org/abstract.cfm?URI=ao-28-22-4735>.
- Mandrake, L., C. Frankenberg, C. O'Dell, G. Osterman, P. Wennberg, and D. Wunch, 2013: Semi-autonomous sounding selection for OCO-2. *Atmos. Meas. Tech.*, **6**, 2851–2864, doi:10.5194/amt-6-2851-2013.
- O'Dell, C. W., et al., 2012: The ACOS CO<sub>2</sub> retrieval algorithm–Part 1: Description and validation against synthetic observations. *Atmos. Meas. Tech.*, **5**, 99–121, doi:10.5194/amt-5-99-2012.